FULL PAPER

ADVANCED FUNCTIONAL MATERIALS

DOI: 10.1002/adfm.200700350

Hydrolytically Stable Phosphorylated Hybrid Silicas for Proton Conduction**

By *Yonggang Jin*, *Shizhang Qiao*, *João C. Diniz da Costa*, *Barry J. Wood*, *Bradley P. Ladewig*, and *Gao Qing Lu**

A new approach to the synthesis of fully immobilized phosphorus functionalized hybrid proton conductive gels based on phosphonic acid grafting is presented in this paper. The hybrid silicas with different amounts of phosphonic acid have been prepared and characterized using Fourier-transform infrared spectroscopy, X-ray photoelectron spectroscopy, Brunauer–Emmett–Teller surface area analysis, thermogravimetric analysis, and electrochemical techniques. The proton conductivity of the materials depend strongly on hydration, which increases by four orders of magnitude over the relative humidity (RH) range of 20 to 100 %, up to a maximum of 0.027 S cm^{-1} at 100 °C and 100 % RH. For the reported samples, proton conduction is believed to occur within a dynamic hydrogen-bond network formed by functionalized P–OH groups and water molecules by the Grotthuss mechanism. However, the proton conductive sites (P–OH) are likely to be partially immobilized by strong protonic receptors (N atoms in amines), which reduces the free P–OH groups and restricts proton transfer. Hydration may cause a bonding structural rearrangement, which results in more free P–OH groups as active proton conductive sites and, therefore, greatly increased proton conductivity is observed.

1. Introduction

Fuel cell technologies have attracted much attention in the last few years as an efficient and clean alternative to traditional combustion to generate electricity.[1–4] Among fuel cell types, the proton exchange membrane fuel cell (PEMFC) is the most popular for transport applications and as a small portable power source.[5] The proton exchange membrane (PEM) is a key component of a PEMFC, which divides the oxidation and reduction reactions between the anode and the cathode, as well as allowing protons to pass through the membrane to complete the entire reaction.[6]

The current technology for PEMFCs, based on perfluorosulfonic acid polymer membranes operating at a typical temperature of 80 °C is limited by its inability to operate at intermediate temperatures above 100 °C, where a number of advanced features, e.g., high CO poisoning tolerance, and simple thermal and water management can be attained.[7–9] Hence, the search for a thermally stable and highly proton conductive material for use as a PEM is highly desirable. In recent years, more research efforts have focused on solid acid proton conductive materials (e.g., zirconium, titanium, and silicon phosphates) as an alternative to polymer PEMs.[10] These materials, which consist of an inorganic oxide network and functionalized phosphates, exhibit excellent thermal stability and suitable proton conductivity especially at high operating temperatures above 100 °C. On the other hand, these materials were prepared by a sol–gel route, a synthetic process that offers much flexibility to tune the structure of final products and adjust the composition of functional groups. Of these materials, silicon phosphates showed the most promise with proton conductivities above 100 °C and in dry conditions. Silicon phosphate gels with a high amount of phosphorus have been extensively studied by Matsuda et al.[11–15] for their proton conductivity at the low to high temperature and a wide relative humidity (RH) range. It has been hypothesized that proton conduction in silicon phosphate gels mainly results from proton hopping by hydroxy groups in the phosphate (i.e., P–OH) and water molecules through a Grotthuss mechanism. Furthermore, the gels have a strong affinity to water molecules because of the strong hydrogen bonding between P–OH and water, which results in the need for a much higher temperature than 100 °C to remove water molecules. This is the reason why the gels show high proton conductivities even at a high temperature and low RH. An experimental value as high as 0.01 S cm^{-1} at 150 °C and 0.4 % RH has been reported.[11] However, P–O–Si bonds in gels are not stable towards hydrolysis,[16] which results in free phosphoric

[*] Prof. G. Q. (Max) Lu, Y. G. Jin, Dr. S. Z. Qiao, Dr. J. C. D. da Costa, Dr. B. P. Ladewig
ARC Centre of Excellence for Functional Nanomaterials
Australian Institute of Bioengineering and Nanotechology
The University of Queensland
QLD 4072 (Australia)
E-mail: maxlu@uq.edu.au
Dr. B. J. Wood
Brisbane Surface Analysis Facility
The University of Queensland
QLD 4072 (Australia)

[**] The authors acknowledge the financial support for this project from the Australian Research Council and the ARC Federation Fellowship (to Prof. G. Q. Lu).

ADVANCED FUNCTIONAL MATERIALS

acid after the gels are hydrolyzed by water. Resultant free acid will leach out in the use of the fuel cell, which causes a rapid drop of conductivity during the operation. To attempt to improve chemical stability, silicon phosphate gels were synthesized with the addition of a third component such as Al_2O_3, B_2O_3, and TiO_2, with the aim to stabilize the phosphates by forming hydrolytically stable bonds between the third component and the phosphate.[17] The results showed that conductivities decreased by over two orders of magnitude compared to those of binary silicon phosphate gels. Therefore, how to improve the hydrolytic stability between phosphorus functional groups and silica backbones becomes a key issue for the development of phosphorus-functionalized silica proton conductive materials.

Very recently, a few papers have been published with regards to proton conductive hybrid silica membranes based on phosphonic acid. In the work of Binsu et al,[18] the stable phosphorylation was realized using aminopropyltriethoxysilane (APTES), formaldehyde, and phosphorous acid by the Kabachnik–Fields (K-F) reaction,[19,20] which resulted in covalently bonded $Si(CH_2)_3$–N–C–P groups. Furthermore, Li et al.[21] utilized other interesting molecular precursors (e.g., diethoxyphosphoryl ethyltriethoxysilane) to introduce phosphonic acid groups into a silicate hybrid network by the Si–C and P–C bonds. In both works above, the Si–C and P–C bonds were involved to overcome the instability problem of the P–O–Si bonds upon exposure to water. The Si–C and P–C bonds have excellent stability; no leverage is observed under hydrolytic, basic, and acidic conditions.[22–25] Herein, we report a new sol–gel route to synthesize proton conductive hybrid silicas with stable phosphonic acid functionalization. This paper attempts to study the stable phosphorylation, investigate the increased functionalization for improved proton conductivity, and elucidate the proton conduction mechanism involved in this system. In doing so we demonstrate that the prepared hydrolytically stable phosphorylated hybrid silicas are capable of proton conduction at intermediate temperatures.

2. Results and Discussion

A two-step process was employed for the synthesis of phosphorus-functionalized hybrid silicas. In the first step, hybrid silicas that contain primary amino groups were synthesized by the copolycondensation of tetraethoxysilane (TEOS) and APTES in a sol–gel method. The subsequent phosphorylation based on the K-F reaction was conducted by refluxing the obtained amino-containing hybrid silicas with a mixture of formaldehyde and phosphorous acid. A representative reaction scheme is presented in Figure 1. The amino-containing hybrid silicas before phosphorylation are named by the molar ratios of APTES/TEOS = 1/4, 1/2, and 2/3 as 1A4T, 1A2T, and 2A3T, respectively, whereas the phosphorylated samples are distinguished by the letter P, i.e., 1A4TP, 1A2TP, and 2A3TP. In the sol–gel synthesis of hybrid silicas, APTES plays an important role because it acts as a strong base to promote the inorganic polymerization.[26] For example, in the case of sample 1A2T a

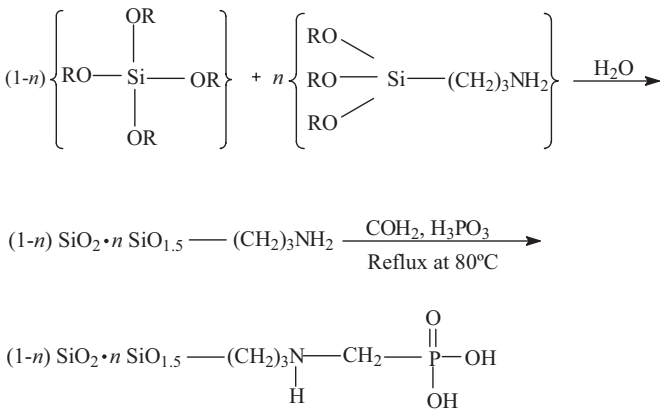

R=C_2H_5; n=1/5, 1/3 and 2/5.

Figure 1. Reaction scheme for phosphorylated hybrid silicas.

transparent gel was formed 6–8 min after the addition of APTES. To attempt to incorporate more amino groups into the hybrid silicas, the samples with APTES/TEOS = 1/1 and 3/2 were also prepared. However, the appearance of a condensed compound took longer in both samples than those containing less APTES, and a phase separation was observed in their final dried samples. Furthermore, at the second stage of the reaction, both solid samples dissolved during refluxing. It is well known that the trifunctional alkoxides preferentially yield small condensed units (i.e., cyclic oligomers that contain several monomer units) as sol–gel reactions proceed.[27–29] Hence, the gelation should be absent for APTES alone. This suggests that the presence of TEOS as a crosslinking agent is necessary to build a three-dimensional network with APTES and to form a highly condensed compound. To test the hydrolytic stability of the phosphorylated samples, a portion of sample 2A3TP was autoclaved with water at 100 °C for 24 h. The sample subjected to such a hydrothermal treatment is referred to as 2A3TPW.

2.1. Structural Characterization

2.1.1. Fourier-Transform Infrared (FTIR) Spectra

The FTIR spectra for the samples are shown in Figure 2. Sample 2A3T as a representative hybrid silica before phosphorylation shows the asymmetric and symmetric C–H stretching modes in CH_2, respectively, at 2930 and 2865 cm^{-1}.[30] CH_2 deformation vibration modes can also be found at 1470 and 700 cm^{-1}.[30] The appearance of primary amino groups $–NH_2$ can be seen from the weak absorption bands at 3360 (asymmetric stretch) and 3290 cm^{-1} (symmetric stretch), and scissor vibrations at 1595 and 1560 cm^{-1}.[31,32] The absorption bands at 1018, 778, and 428 cm^{-1} are assigned to the Si–O–Si asymmetric stretch, Si–O–Si symmetric stretch, and Si–O–Si bend, respectively.[30,33] This indicates that a hydrolysis and condensation reaction occurred between TEOS and APTES by a sol–gel process to form the silicate network structure. An absorption shoulder at 944 cm^{-1} arises from the Si–O stretch of silanol groups Si–OH.[30] A broad absorption band between 3000–

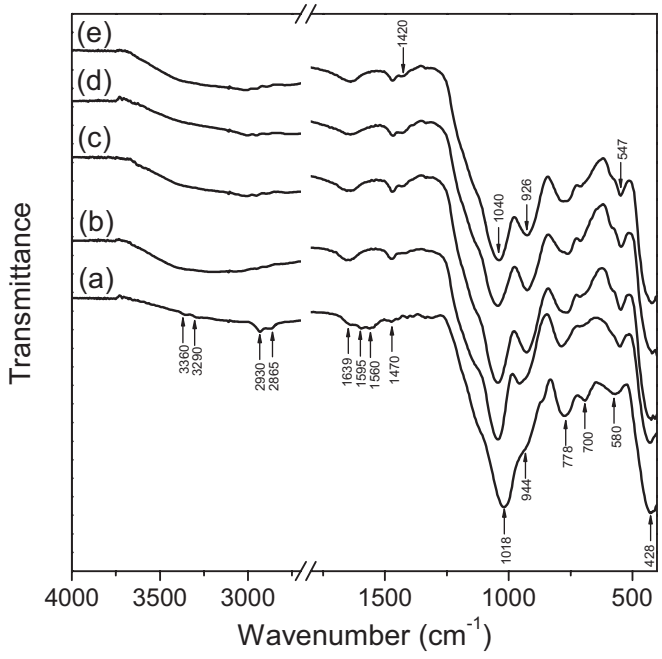

Figure 2. FTIR spectra of a) 2A3T, b) 1A4TP, c) 1A2TP, d) 2A3TP, and e) 2A3TPW.

3700 cm^{-1} and an absorption peak at 1639 cm^{-1} are attributed to the stretch mode of O–H and the bend mode of absorbed water molecules, respectively. A week absorption band at 580 cm^{-1} may be assigned to the O–Si–O vibration of incompletely hydrolyzed TEOS and APTES.[33]

Compared to the spectrum of 2A3T, the spectra of the phosphorylated samples show three distinct changes. First, the bands of the primary amino groups (3360, 3290, 1595, and 1560 cm^{-1}) have disappeared, which suggests that phosphonomethylation of the amino groups may occur when refluxing in the mixture of formaldehyde and phosphorous acid. This can be proven by the appearance of the C–H vibration band (1420 cm^{-1}) of the *N*-phosphomethylated fragments ($CH_2PO(OH)_2$),[32] the intensity of which increases with an increase in the addition of APTES. Moreover, the intensity of the band that corresponds to CH_2 (1470 cm^{-1}) increases, which indicates an increase in the amount of CH_2 after the phosphorylation reaction. Second, the bands assigned to the P–O stretch (926 cm^{-1}) and bend (547 cm^{-1}) appear in the phosphorylated samples,[30] while the intensity increases with the amount of amino groups. The absorption band of the P=O group (1140–1240 cm^{-1}) is overlapped by the absorption bands of the silica backbone and thus is unobserved. Interestingly, the hydrothermally treated sample 2A3TPW has a similar FTIR spectrum to that before treatment, and a decrease in the intensity of the absorption peaks assigned to the phosphonic acid groups cannot be seen. This would suggest that a hydrolytically stable phosphorylation has been successfully achieved through the K-F reaction in the present work. Finally, the broad Si–O–Si asymmetric band (1040 cm^{-1}) shifts and the shoulder assigned to Si–OH disappears, which may be attributed to the effect of incorporated phosphonic groups. In addition, the band at 580 cm^{-1} is presented as a shoulder because of the overlap of strong P–O absorption band at 547 cm^{-1}.

2.1.2. X-ray Photoelectron Spectroscopy (XPS)

The survey XPS spectra of three phosphorylated samples are shown in Figure 3 along with that of 2A3T for comparison. The intense P1s and P2p peaks can be seen in all phosphorylated samples, arising from functionalized phosphorus groups. Their intensity increases with the increase in the addition of APTES during the synthesis. Table 1 lists the elemental composition of the amino-containing, phosphorylated and hydrothermally treated samples obtained from XPS spectra curve fitting. It can be seen that reasonable values of both nitrogen and silicon are detected in the samples. The atomic ratio of N/Si is proportional to the added amount of APTES, which is in good agreement with the stoichiometric N/Si ratio for the amino-containing hybrid silicas. Strictly speaking, the elemental composition calculated from XPS surface characterization is only valid for homogeneous samples to accurately reflect the entire composition. The reasonable N/Si ratios reveal that sol–gel derived hybrid silicas are homogeneous in atomic distribution.

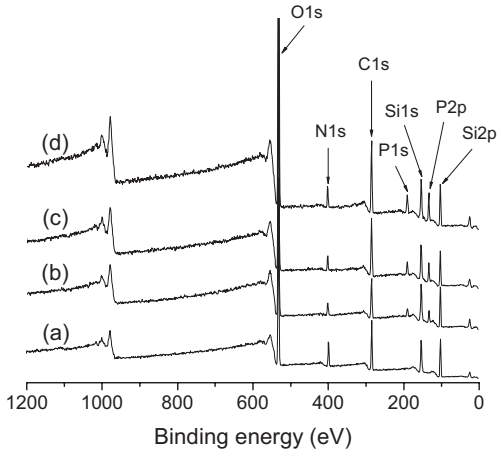

Figure 3. Survey XPS spectra of a) 2A3T, b) 1A4TP, c) 1A2TP, and d) 2A3TP.

Table 1. Elemental composition obtained from XPS analysis.

Sample	Element content [at %]					Atomic ratio		
	O	N	C	Si	P	N/Si	P/Si	P/N
1A4T	50.44	5.01	23.06	21.49	0	0.23	0	0
1A2T	44.63	6.86	27.12	21.39	0	0.32	0	0
2A3T	40.18	8.39	31.2	20.22	0	0.41	0	0
1A4TP	50.16	4.19	23.86	19.07	2.7	0.22	0.14	0.64
1A2TP	49.62	4.1	26.59	15.12	4.58	0.27	0.30	1.12
2A3TP	55.01	3.91	25.16	11.25	4.66	0.35	0.41	1.19
2A3TPW	54.59	4.11	24.1	12.47	4.73	0.33	0.38	1.15

ADVANCED FUNCTIONAL MATERIALS

FULL PAPER

For the phosphorylated silicas, the N/Si ratio reduces after phosphorylation, especially for the sample with a high amount of APTES (i.e., 2A3TP). This is likely a result of the loss of incompletely hydrolyzed and condensed APTES during the second synthesis stage. The content of phosphorus is higher in the sample with a larger amount of APTES because the amino group is the only functional site that anchors the phosphonic acid. The ratios of P/Si determined by XPS analysis show the conversion of amine ($-NH_2$) to aminophosphonic groups ($-N-C-PO(OH)_2$) for 1A2T and 2A3T is about 1.1–1.2 in terms of the molar ratio of P/N, whilst a lower conversion at 0.64 is observed for 1A4T. Hence, 1A4T is essentially less modified with a lower phosphorus functionalization. The reason for this is unclear at the moment, but probably results from the different textile structures of the hybrid silicas with varied amounts of APTES. Among the three samples, 1A4T has the highest Brunauer–Emmett–Teller (BET) surface area of 255 $m^2 g^{-1}$, whereas the BET surface area is 123 and 87 $m^2 g^{-1}$ for 1A2T and 2A3T, respectively. A similar phenomenon was reported by Zaitsev et al.[25] who studied the surface modification of silicas with various porous structures by aminophosphonic acids and concluded that the mesoporous silica with a higher surface area reached a lower phosphorus yield at the second stage of reaction. Furthermore, the P/N value is not as high as it is expected since two phosphonic acid molecules should be grafted onto each amino group, thus P/N is supposed to be around 2. This may be either caused by a side reaction that occurs by the condensation of two neighbouring amines with a formaldehyde molecule or attributed to the fact that the primary amines are more reactive than the secondary amines in the K-F reaction.[25] In our work, a large excess amount of phosphorous acid and formaldehyde was used compared to the amino content in the hybrid silicas. The phosphorus conversion should be improved or optimized by adjusting the molar ratio of starting components in the second stage of the synthesis. In addition, a hydrolytically stable phosphorylation has been confirmed in the present work based on the XPS results for 2A3TPW (see Table 1). It can be seen that the phosphorus content does not reduce very much after a rigorous hydrothermal treatment.

Shown in Figure 4 are the C1s spectra of sample 2A3T and its phosphorylated counterpart 2A3TP. For 2A3T, three strong peaks at 284.3, 285, and 285.8 eV can be assigned to C–Si, C–C/C–H and C–N in aminopropyl groups of APTES.[34,35] The peak areas of C–N and C–Si are almost equivalent as determined by curve fitting, 666 versus 679, which is very close to the stoichiometric ratio of N/Si = 1 in APTES molecules. In addition to the three peaks, the appearance of a small peak at 286.8 was not expected. The presence of this peak most probably originates from C=O bonds as a result of contamination.[36] The four peaks observed for 2A3T can also be seen on phosphorylated sample 2A3TP, but with different intensities. The intensity of the C–N peak (286.1 eV) for 2A3TP is much stronger than that for 2A3T. This suggests that the K-F reaction has occurred and the resultant C–N bonds are a result of the nucleophilic addition of amines to formaldehyde. Of course, the side reaction of two neighbouring amines condensing with a formaldehyde molecule cannot be ruled out. However, as far as the excellent stability of phosphorus on 2A3TPW is concerned, phosphonic acid groups are certain to be attached to the hybrid silica network by the K-F reaction by covalent bonds of N–C–P.

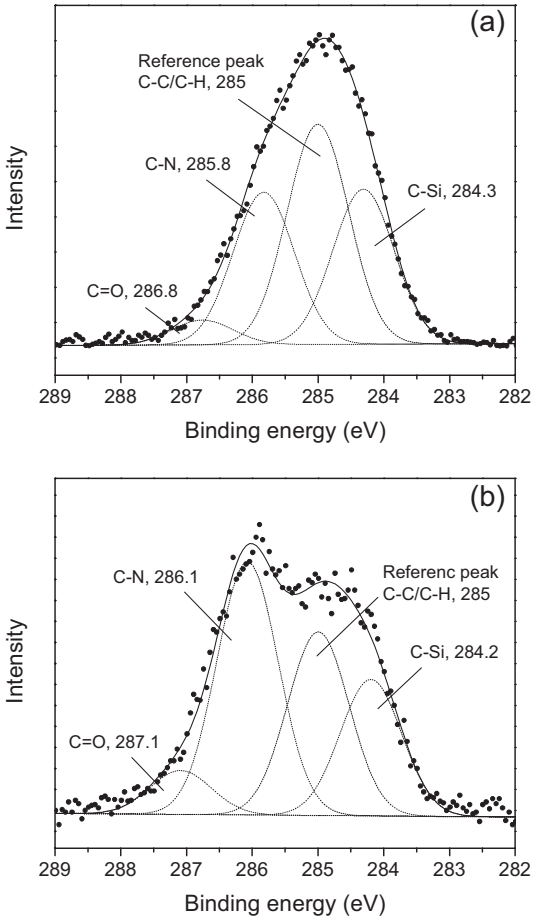

Figure 4. C1s XPS spectra of a) 2A3T and b) 2A3TP.

Figure 5 shows the N1s spectra of sample 2A3T and 2A3TP. Two peaks can be seen for 2A3T. One with a high intensity at 399.3 eV should be attributed to primary amines ($C-NH_2$),[34,37] the other one with a much lower intensity is located at 400.7 eV, which is close to the bonding energy reported for imides at 400.5 eV.[34] Thus, the latter peak should be assigned to imide groups probably present as a result of contamination as has been seen for the C1s peak at 286.8 eV. However, 2A3TP only presents an intense peak at 401.9 eV, which corresponds to quarternary N species.[34,35] Such a bonding structure should result from the protonation of N species, which is most probably caused by hydrogen bonds between P–OH groups of grafted phosphonic acid and N atoms of amino groups as strong protonic receptors that have a very low K_a ($\sim 10^{-10}$) of $-NH_3^+/-NH_2$.[38] Hence, phosphorylated hybrid silicas are supposed to be networked by a strong hydrogen-bonding interaction. The samples with the other two compositions had a similar peak fitting to 2A3T and 2A3TP.

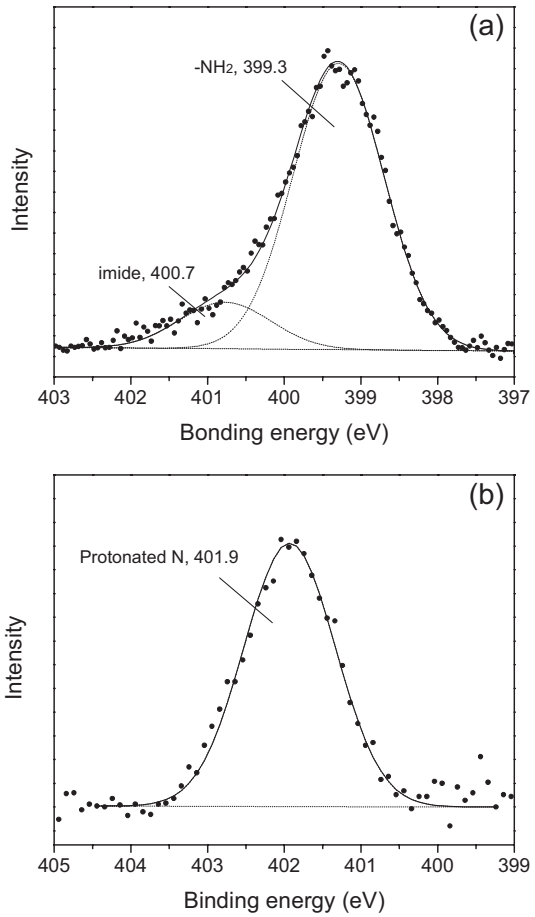

Figure 5. N1s XPS spectra of a) 2A3T and b) 2A3TP.

2.2. Thermal Stability

Thermogravimetric analysis (TGA) was carried out on sample 2A3T and 2A3TP to examine their thermal stability for an intermediate temperature PEM application. The TG curves and their corresponding derivative (DTG) curves for both samples are presented in Figure 6. For 2A3T, the 5 % weight loss at 150–420 °C is likely a result of the loss of a small amount of strongly adsorbed water and the dehydroxylation of silicate networks. A large weight loss of 17 % at 420–700 °C should be attributed to the decomposition of aminopropyl groups incorporated in the hybrid silica. The DTG curve shows two peaks in this temperature region, which indicates that the aminopropyl groups may be decomposed stepwise upon heating. For phosphorylated sample 2A3TP, the first weight loss peak at 150–350 °C, which presents a broad DTG peak, is mainly caused by dehydration of phosphonic acid by combining two P–OH groups to produce a water molecule. Like 2A3T, a large weight loss of about 14 % at 350–630 °C follows, which should be attributed to the decomposition of organic groups. With regards to the decomposition temperatures, the incorporation of phosphonic acid reduced the thermal stability of the hybrid silica. In addition, this part of weight loss in 2A3TP is less than that of 2A3T. This may be attributable to the phosphonic acid reacting to form phosphate or phosphorus oxides to remain in the materials. In addition, both samples exhibit 1–2 % weight loss in the final phases of weight loss. This is probably because of the continuous dehydroxylation of the silicate networks. Thus, the phosphorylated silica 2A3TP is thermally stable up to 350 °C and may be suitable for the use in the intermediate temperature range of 100–200 °C for PEMFCs.

2.3. Proton Conduction

The conductivity of the phosphorylated samples as a function of RH at 100 °C is shown in Figure 7. The conductivity changes from 8.2×10^{-6} S cm^{-1} at 20 % RH to 0.027 S cm^{-1} at 100 % RH for 2A3TP, while 1A2TP exhibits a lower conductivity that ranges from 1.7×10^{-6} to 0.014 S cm^{-1} over the same humidity range. Thus, the results reveal that proton conductivity strongly depends on humidity for both samples. The strong dependence of conductivity on hydration clearly indicates that absorbed water is facilitating proton conduction. This suggests that absorbed water molecules may bridge the functional phosphonic acid groups for proton transfer. In addition, bonding structural changes have been reported in a previous study,[25] where the

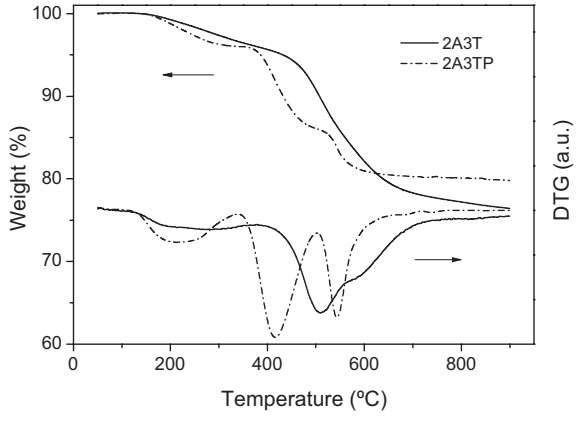

Figure 6. TG and derivative curves for 2A3T and 2A3TP.

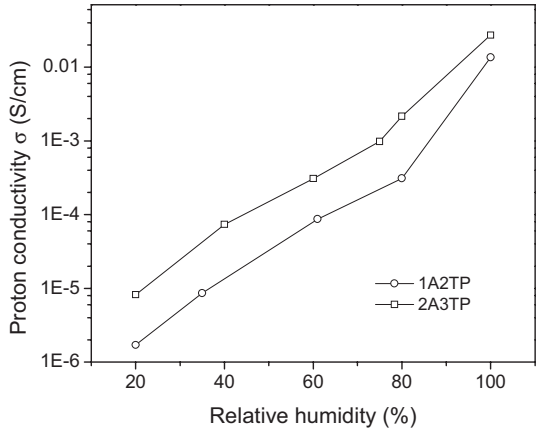

Figure 7. Proton conductivity of 1A2TP and 2A3TP as a function of RH at 100 °C.

ADVANCED FUNCTIONAL MATERIALS

hydrogen bonds between aminophosphonic groups and silanol groups found in air-dried aminophosphonic acid grafted silicas were broken off upon hydration, based on the NMR spectra. In our dehydrated samples, the functionalized P–OH groups are believed to be restricted by hydrogen bonds with amino groups. Therefore, it is postulated that a similar bonding structural rearrangement could occur in the case here. In the highly hydrated sample, the interactions between P–OH and amino groups were relaxed after adsorbing a large amount of water molecules, to result in more free P–OH groups for proton conduction. Hence an increase of proton conductivity up to four orders of magnitude was observed in fully hydrated samples.

Figure 8a shows the conductivity results of samples as a function of increasing temperature at 100 % RH and the conductivity of a Nafion 117 membrane as measured in our laboratory under the same conditions. After phosphorylation, sample 1A2T shows over 1–2 order(s) of magnitude conductivity increase across the entire temperature range. Like pure silicas, the slow proton conduction observed for 1A2T is supposed to result from proton transfer between weakly protongenic Si–OH groups and water molecules.[39,40] As shown by Figure 8a, the conductivity increases with the increase in the content of APTES in hybrid silicas, where more phosphonic acid groups have been incorporated as confirmed by XPS analysis. Sample 2A3TP has the highest conductivity of all three phosphorylated samples, and is only about one times lower than Nafion 117. As an example, the corresponding complex impedance Nyquist plots for 2A3TP are presented in Figure 8b. It can be seen that the intercept of the impedance curve on the real axis decreases as the test temperature increases. This gives a clear indication of the higher resistance to proton conduction at a lower temperature. Despite the fact that the conductivity of the reported sample is not as high as for Nafion, the conductivity result is still promising when it is considered that Nafion membranes cannot operate at this temperature because of glass transition temperature limitations.[10,41] It must also be noted that our maximum test temperature was limited to 100 °C because of equipment limitations. As 2A3TP is thermally stable up to 350 °C as show by TGA, it is anticipated that it would be continuously well conductive in a saturated environment above 100 °C. In addition, the thermal stability of proton conduction of the phosphorylated silica was examined by re-measuring the conductivity after 2A3TP was heated in air at 200 °C for 8 h. The reason for choosing 200 °C is that PEMFC is expected to operate in the intermediate temperature range 100–200 °C. The conductivity was found to be quite stable after heat treatment and a value of 0.025 S cm^{-1} was obtained at 100 °C and 100 % RH, with the conductivity being similar to that of its unheated sample under similar conditions (0.027 S cm^{-1}). The agreement between two values confirms that the organic groups (Si–propyl–N–C–P) of the hybrid silica are thermally stable up to a minimum temperature of 200 °C. The result would be supported by the reported thermal stability of the Si–alkylsulfonic groups presented in the mesoporous silica that was found intact after the sample was calcined at 300 °C in air.[42] Based on the TGA results, the dehydration of two P–OH groups to form a P–O–P group should occur during heat treatment at 200 °C. However, the reaction could be reversed by hydration in a 100 % RH testing atmosphere.

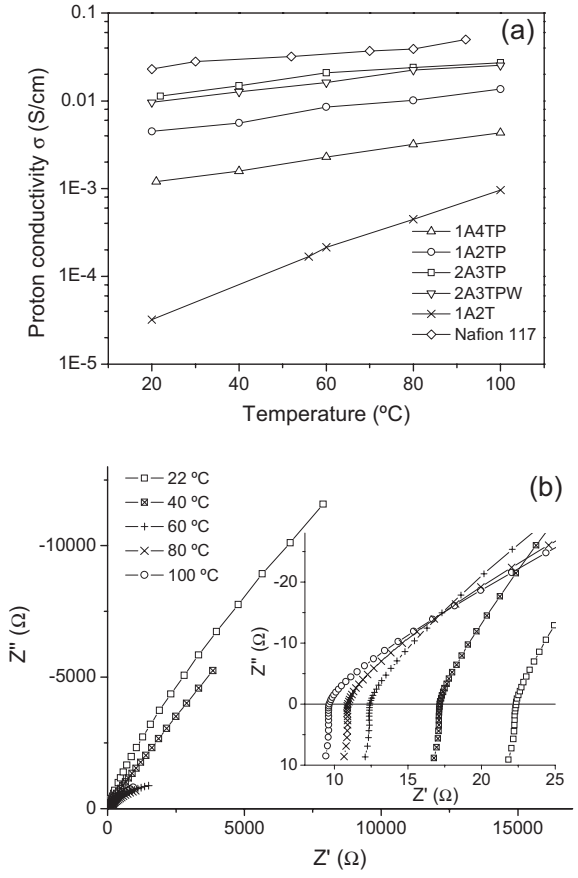

Figure 8. a) Proton conductivity of 1A2T, 1A4TP, 1A2TP, 2A3TP, 2A3TPW, and a Nafion 117 membrane as a function of temperature at 100 % RH. The corresponding complex impedance Nyquist plots for 2A3TP are presented in (b). The inset shows the intercept of each plot on the real axis.

Most interestingly, the conductivity of 2A3TPW is only slightly less than that of 2A3TP, which suggests that the phosphorylation method based on the K-F reaction successfully immobilized functional phosphonic acid groups into the silicate network so that the synthesized samples would be stable in a fuel cell that operates over an extended period of time. The reason for a slight decrease of conductivity after hydrothermal treatment is most probably a result of the loss during boiling of some incompletely hydrolyzed and condensed APTES molecules that have been grafted with phosphonic acid at the second synthesis stage. It can be seen from Table 1 that a slight decrease in not only the atomic ratio of P/Si, but also that for N/Si is observed after the hydrothermal treatment.

The value of the activation energies (E_a) for each of the phosphorylated samples was calculated using the Arrhenius equation $\sigma = \sigma_0 \exp(-E_a/kT)$, where σ_0 is a pre-exponential factor, k is the Boltzmann's constant, and the temperature T is in Kelvin. Figure 9 shows the Arrhenius plot of the conductivities of each of the samples. It can be seen that an increase in phosphorus concentration results in a decrease of activation energy ranging from 0.11–0.16 eV. The smaller activation energy facili-

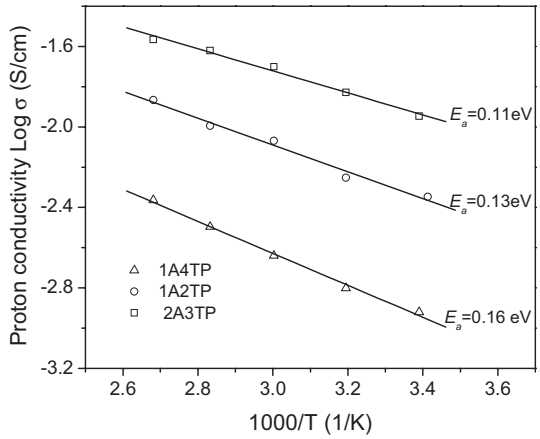

Figure 9. Proton conductivity Arrhenius plots of 1A4TP, 1A2TP, and 2A3TP as a function of temperature at 100 % RH.

tates easier proton transfer. At a molecular level the proton conduction in PEMs is discussed in the view of a vehicle (diffusion) mechanism and a Grotthuss (hopping) mechanism.[43,44] In the vehicle mechanism, the protons diffuse together with solvent molecules by forming a complex such as $H_5O_2^+$ and $H_9O_4^+$. In the Grotthuss mechanism, however, the protons jump from one solvent molecule or functional group to the next by the continuous formation and breaking of hydrogen bonds. This mechanism preferentially occurs in acid-containing systems with an activation energy of 0.1–0.4 eV.[44,45] The activation energy estimated for the phosphorylated samples falls within this range. Hence this would suggest that the proton conduction in the phosphorylated samples may occur by a Grotthuss mechanism and is enhanced by the presence of grafted phosphonic acid that has free pendant P–OH groups, as shown in Figure 10. These P–OH groups can not only act as active sites to donate or accept protons, but can also network water molecules by hydrogen bonds to provide a continuous proton conduction pathway. Thus, an enhancement of proton conductivity was observed for the sample with a higher phosphorus content and more absorbed water. In addition, the dependence of conductivity on humidity of up to four orders of magnitude in the 20–100 % RH range, may be explained as follows. When the sample is dehydrated (case a in Figure 10), the strong interactions between the amino and P–OH groups reduce the amount of free P–OH groups, as normally every phosphorus should have two pendant P–OH groups in a phosphonic acid molecule. Once hydrated, there may be a bonding structural rearrangement, which would relax the bonding restriction between N and P and result in more free pendant P–OH groups. Thus more pathways and sites for proton conduction would be provided as illustrated by case b in Figure 10.

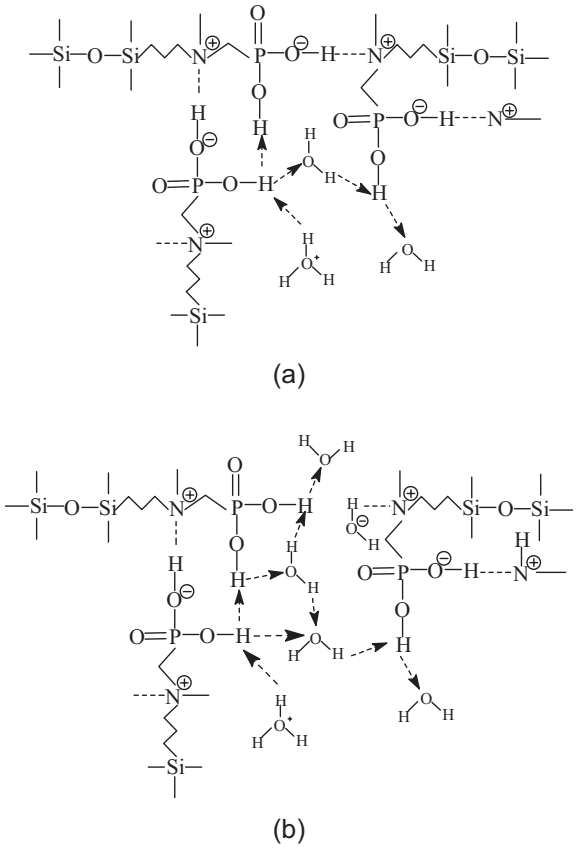

Figure 10. Scheme of the proposed proton conduction mechanism of phosphorylated samples in the a) dehydrated and b) hydrated case.

3. Conclusions

Sol–gel derived hybrid silicas with hydrolytically stable phosphonic acid functionalization are promising solid proton conductors under near saturated humidity conditions at intermediate temperatures above 100 °C. The sample with the largest incorporation of phosphonic acid showed the highest proton conductivity of 0.027 S cm^{-1} at 100 °C and 100 % RH, and good thermal stability up to 350 °C. The hydrolytic stability of phosphorylation was investigated by the hydrothermal treatment at 100 °C for 24 h. The fully immobilized phosphorus functionalization has been confirmed by FTIR spectra, XPS analysis, and conductivity measurements. The proton conduction was found to be dominated by a Grotthuss mechanism, where the functionalized P–OH groups transfer protons in the presence of water. The strong hydrogen bonding between the amino and P–OH groups was supposed to reduce free pendant P–OH groups and thus restrict the proton conduction. Such a restriction could be relaxed by hydration, which leads to an improvement in the proton conductivity. This may explain the strong dependence of conductivity on humidity of up to four orders of magnitude in 20–100 % RH. Further work, such as examining the proton conductivity above 100 °C, fabricating a self-standing organic–inorganic composite membrane that contains this novel hybrid silica proton conductor, and performing fuel cell tests, will be carried out to confirm the suitability for the application to intermediate temperature PEMFCs.

ADVANCED FUNCTIONAL MATERIALS

4. Experimental

The synthesis of amino-containing hybrid silicas followed a similar route to that reported by Yatluk et al. [46]. Briefly, a certain amount of TEOS was measured into a beaker and was placed into an ice bath. To this solution, distilled water was added dropwise for 5 min while stirring. An appropriate amount of APTES was then added to the mixture. The mixture was stirred until the onset of gel formation, and was left for 24 h at room temperature. The formed gel was powdered and dried at 100 °C for 24 h. The molar ratios employed were APTES/TEOS = 1/4, 1/2, and 2/3, and herein the amount of water was added in the molar ratio of H_2O/total Si content = 2/1. The phosphorylation was conducted as follows: 2 g of the hybrid silica obtained was dispersed into a solution of formaldehyde (15 g, 37 wt % in aqueous solution) and phosphorous acid (15 g). The mixture was refluxed for 6 h at 80 °C and then cooled to room temperature. The resulting mixture was then washed with copious amounts of water and centrifuged. This strict washing process was repeated four times, and the obtained powder was dried at 100 °C to constant weight. In the hydrothermal treatment for investigating the hydrolytic stability of phosphorylated samples, a portion of sample 2A3TP was autoclaved with water at 100 °C for 24 h. It was then cooled to room temperature, centrifuged, and dried at 100 °C.

FTIR spectra were collected on a Nicolet 6700 with a resolution of 4 cm^{-1} by using attenuated total reflectance (ATR) techniques. XPS was performed on a Kratos Axis Ultra with a monochromatic Al K_α X-ray source. Each analysis started with a survey scan from 0 to 1200 eV with a dwell time of 100 ms, pass energy of 160 eV at steps of 1 eV with 1 sweep. For the high-resolution scans of selected elements, the number of sweeps was increased, the pass energy was lowered to 20 eV at steps of 100 meV, and the dwell time was changed to 250 ms. C1s with a binding energy of 285 eV was used as the reference. N_2 adsorption measurements were conducted on a Quantachrome Instruments Quadrasorb SI at liquid nitrogen temperature. The specific surface areas of the samples were calculated using the multiple-point BET method in the relative pressure range $P/P_0 = 0.05$–0.3. The thermal stability of the samples was investigated by TGA, which was carried out using a Shimadzu TGA 50H at a heating rate of 10 °C min^{-1} under nitrogen atmosphere. Prior to the tests, samples were kept in an oven at 100 °C for 6 h.

Proton conductivity measurements were made using a Solartron 1260 Frequency Response Analyzer. Sample pellets of 13 mm diameter were prepared by pressing approximately 200 mg of material for 3 min at 150 kg cm^{-2}. The sample was placed between two gold-plated blocking electrodes of 0.5 cm^2 area in a chamber. The RH was precisely controlled by feeding a mixture of humidified and dry air to the chamber, the relative flows of which were adjusted according to the humidity measured adjacent to the sample using a humidity sensor. For 100 % RH experiments a small quantity of water was placed in the sealed chamber, so that the test atmosphere was at equilibrium with the liquid water. Similarly, the temperature of the chamber was carefully controlled and independently measured adjacent to the sample using a thermocouple. After achieving equilibrium at each temperature and RH condition, the sample impedance was measured over the frequency range 10 MHz to 1 Hz at an amplitude of 10 mV. The proton conductivity, σ (S cm^{-1}), was defined as $\sigma = l/[(R - R_0)A]$, where l is the sample pellet thickness (cm), A is the electrode contact area (0.5 cm^2 in the current cases), R the tested sample resistance (taken as the impedance at zero phase angle, Ω), and R_0 is the rig short circuit resistance (Ω).

Received: March 25, 2007
Revised: July 26, 2007
Published online: September 20, 2007

[1] K. Ledjeff-Hey, V. Formanski, T. Kalk, J. Roes, *J. Power Sources* **1998**, *71*, 199.
[2] W. Smith, *J. Power Sources* **2000**, *86*, 74.
[3] G. Erdmann, *Int. J. Hydrogen Energy* **2003**, *28*, 685.
[4] L. F. Brown, *Int. J. Hydrogen Energy* **2001**, *26*, 381.
[5] L. Carrette, K. A. Friedrich, U. Stimming, *ChemPhysChem.* **2000**, *1*, 162.
[6] V. Mehta, J. S. Cooper, *J. Power Sources* **2003**, *114*, 32.
[7] Q. F. Li, R. H. He, J. O. Jensen, N. J. Bjerrum, *Chem. Mater.* **2003**, *15*, 4896.
[8] K. A. Mauritz, R. B. Moore, *Chem. Rev.* **2004**, *104*, 4535.
[9] B. Smitha, S. Sridhar, A. A. Khan, *J. Membr. Sci.* **2005**, *259*, 10.
[10] W. H. J. Hogarth, J. C. D. da Costa, G. Q. Lu, *J. Power Sources* **2005**, *142*, 223.
[11] A. Matsuda, T. Kanzaki, K. Tadanaga, M. Tatsumisago, T. Minami, *Electrochim. Acta* **2001**, *47*, 939.
[12] A. Matsuda, T. Kanzaki, M. Tatsumisago, T. Minami, *Solid State Ionics* **2001**, *145*, 161.
[13] A. Matsuda, T. Kanzaki, Y. Kotani, M. Tatsumisago, T. Minami, *Solid State Ionics* **2001**, *139*, 113.
[14] A. Matsuda, T. Kanzaki, K. Tadanaga, M. Tatsumisago, T. Minami, *Solid State Ionics* **2002**, *154*, 687.
[15] A. Matsuda, T. Kanzaki, K. Tadanaga, M. Tatsumisago, T. Minami, *J. Ceram. Soc. Jpn.* **2002**, *110*, 131.
[16] N. J. Clayden, A. Aronne, S. Esposito, P. Pernice, *J. Non-Cryst. Solids* **2004**, *345*, 601.
[17] A. Matsuda, Y. Nono, K. Tadanaga, T. Minami, M. Tatsumisago, *Solid State Ionics* **2003**, *162*, 253.
[18] V. V. Binsu, R. K. Nagarale, V. K. Shahi, *J. Mater. Chem.* **2005**, *15*, 4823.
[19] E. K. Fields, *J. Am. Chem. Soc.* **1952**, *74*, 1528.
[20] R. A. Cherkasov, V. I. Galkin, *Russ. Chem. Rev.* **1998**, *67*, 857.
[21] S. W. Li, Z. Zhou, H. Abernathy, M. L. Liu, W. Li, J. Ukai, K. Hase, M. Nakanishi, *J. Mater. Chem.* **2006**, *16*, 858.
[22] G. Alberti, P. Cardini-Galli, U. Costantino, E. Torracca, *J. Inorg. Nucl. Chem.* **1967**, *29*, 571.
[23] G. H. Barnes, M. P. David, *J. Org. Chem.* **1960**, *25*, 1191.
[24] A. Cardenas, N. Hovnanian, M. Smaihi, *J. Appl. Polym. Sci.* **1996**, *60*, 2279.
[25] V. N. Zaitsev, L. S. Vasilik, J. Evans, A. Brough, *Russ. Chem. Bull.* **1999**, *48*, 2315.
[26] C. J. Brinker, G. W. Scherer, in *Sol–Gel Science*: *The Physics and Chemistry of Sol–gel Processing*, Academic Press, Boston **1990**, Ch. 3.
[27] T. C. Kendrick, B. Parbhoo, J. W. White, in *The Chemistry of Organic Silicon Compounds Part 2* (Eds: S. Patai, Z. Rappoport), Wiley, New York **1989**, p. 1290.
[28] M. A. Brook, in *Silicon in Organic*, *Organometallic and Polymer Chemistry*, Wiley, New York **1999**, p. 256.
[29] H. Steininger, M. Schuster, K. D. Kreuer, J. Maier, *Solid State Ionics* **2006**, *177*, 2457.
[30] B. C. Smith, in *Infrared Spectral Interpretation*: *A Systematic Approach*, CRC Press, Boca Raton, FL **1999**, p. 243.
[31] L. D. White, C. P. Tripp, *J. Colloid Interface Sci.* **2000**, *232*, 400.
[32] G. L. Matevosyan, Y. S. Yukha, P. M. Zavlin, *Russ. J. Gen. Chem.* **2003**, *73*, 1725.
[33] S.-P. Tung, B.-J. Hwang, *J. Membr. Sci.* **2004**, *241*, 315.
[34] G. Beamson, D. Briggs, in *High Resolution XPS of Organic Polymers—The Scienta ESCA300 Database*, J. Wiley & Sons, Chichester **1992**.
[35] A. S. M. Chong, X. S. Zhao, *J. Phys. Chem. B* **2003**, *107*, 12650.
[36] E. Tavenner, P. Meredith, B. Wood, M. Curry, R. Giedd, *Synth. Met.* **2004**, *145*, 183.
[37] T. R. Gengenbach, R. C. Chatelier, H. J. Griesser, *Surf. Interface Anal.* **1996**, *24*, 611.
[38] P. L. Kuo, W. F. Chen, W. J. Liang, *J. Polym. Sci., Part A*: *Polym. Chem.* **2005**, *43*, 3359.
[39] M. Nogami, R. Nagao, G. Wong, T. Kasuga, T. Hayakawa, *J Phys. Chem. B* **1999**, *103*, 9468.
[40] M. Nogami, H. Matsushita, Y. Goto, T. Kasuga, *Adv. Mater.* **2000**, *12*, 1370.
[41] S. C. Yeo, A. Eisenberg, *J. Appl. Polym. Sci.* **1977**, *21*, 875.
[42] D. Margolese, J. A. Melero, S. C. Christiansen, B. F. Chmelka, G. D. Stucky, *Chem. Mater.* **2000**, *12*, 2448.
[43] K.-D. Kreuer, *Chem. Mater.* **1996**, *8*, 610.
[44] H. Munakata, H. Chiba, K. Kanamura, *Solid State Ionics* **2005**, *176*, 2445.
[45] P. Colomban, A. Novak, *J. Mol. Struct.* **1988**, *177*, 277.
[46] Y. G. Yatluk, N. A. Zhuravlev, O. V. Koryakova, L. K. Neudachina, Y. A. Skorik, *Russ. Chem. Bull.* **2005**, *54*, 1836.

